ORIGINAL PAPER

Two-Dimensional Materials

physica status solidi b

www.pss-b.com

Growth of Nanocrystalline $MoSe_2$ Monolayers on Epitaxial Graphene from Amorphous Precursors

*Fabian Göhler, Erik C. Hadland, Constance Schmidt, Dietrich R. T. Zahn, Florian Speck, David C. Johnson, and Thomas Seyller**

A new approach to the growth of $MoSe_2$ thin films on epitaxial graphene on SiC(0001) by the use of modulated elemental reactants (MER) precursors has been reported. The synthesis applies a two-step process, where first an amorphous precursor is deposited on the substrate which self-assembles upon annealing. Films with a nominal thickness of about 1 ML are successfully grown on epitaxial graphene monolayer as well as buffer layer samples. Characterization of the films is performed using XPS, LEED, AFM, and Raman spectroscopy. The films are nanocrystalline and show randomly rotated domains. This approach opens up an avenue to synthesize a number of new van-der-Waals systems on epitaxial graphene and other substrates.

1. Introduction

Two-dimensional materials are at the forefront of materials science research, as their unique properties make them enticing for novel applications.[1] Next to graphene, the transition metal dichalcogenides (TMDCs) are of particular interest[2–4] due to their variety of electronic and chemical properties. Recent research efforts have focused on combining different 2D sheets into so called van-der-Waals heterostructures[5] to investigate emergent properties. Heterostructures consisting of $MoSe_2$ and graphene have raised particular interest due to possible applications as catalysts.[6] There are several studies investigating the growth of large area $MoSe_2$ on graphene, either by CVD[7] or MBE.[8–10] Herein, we want to introduce a novel approach to the synthesis of $MoSe_2$ on epitaxial graphene, starting from amorphous elemental precursors. This approach is generally referred to in the literature as the modulated elemental reactants (MER) synthesis.[11,12] The technique is commonly used to grow non-epitaxial intergrowths of metal chalcogenide (MX) and transition metal dichalcogenide (TX_2) layers[13–15] and is therefore intriguing to be used for the synthesis of complex heterostructures on graphene and other substrates. Epitaxial graphene on SiC-(0001) was chosen as substrate, because it is possible to grow high quality graphene layers on a waver scale residing on an insulating or semiconducting substrate, which makes it suitable for device applications.[16] Growth of epitaxial graphene on SiC(0001) is done by thermal decomposition of the SiC substrate. First, a so called buffer layer with a $\left(6\sqrt{3} \times 6\sqrt{3}\right)R30°$ periodicity is formed, which is topologically similar to graphene, but approximately every third carbon is still covalently bound to the underlying Si atoms, which makes it electronically inactive.[17] With higher temperature, a second carbon layer is grown, and a monolayer of graphene resides on the underlying buffer layer.

F. Göhler, C. Schmidt, Prof. D. R. T. Zahn, Dr. F. Speck, Prof. T. Seyller
Institut für Physik
Technische Universität Chemnitz
Reichenhainer Straße 70, D-09126 Chemnitz, Germany
E-mail: thomas.seyller@physik.tu-chemnitz.de

E. C. Hadland, Prof. D. C. Johnson
Department of Chemistry
University of Oregon
Eugene, OR 97401, USA

The ORCID identification number(s) for the author(s) of this article can be found under https://doi.org/10.1002/pssb.201800283.

DOI: 10.1002/pssb.201800283

2. Experimental Section

Epitaxially grown monolayer graphene (MLG) and buffer layer $\left(6\sqrt{3}\right)$ substrates were prepared via ex situ graphitiziation of n-type doped 6H-SiC wafers in argon atmosphere as described by Emtsev et al.[16] and Ostler et al.[18] The SiC wafers first underwent a wet-chemical cleaning procedure and hydrogen etching at 1425 °C, before being annealed in argon at temperatures of 1675 °C for MLG samples and 1475 °C for $6\sqrt{3}$ samples.

An amorphous precursor of elemental molybdenum and selenium layers, with calibrated thicknesses to form one monolayer of $MoSe_2$ upon annealing, was deposited onto the MLG and $6\sqrt{3}$ substrates in a custom built deposition chamber. To prevent oxidation and contamination of the as-deposited precursors, an additional elemental Se layer with a thickness of 50 nm was evaporated on top. As is sketched in **Figure 1**, the precursor is supposed to self-assemble into a crystalline layer of $MoSe_2$ upon annealing at elevated temperatures, whereas excess Se evaporates.

As a reference material, a bulk-like sample of $MoSe_2$ consisting of 24 repetitions of the precursor was deposited onto a silicon substrate and annealed in inert atmosphere. To prepare a clean surface for investigation of this sample in UHV, the reference sample had to be cleaved at the van-der-Waals gap between adjacent layers. Therefore, the sample was mounted onto the sample holder between two steel plates

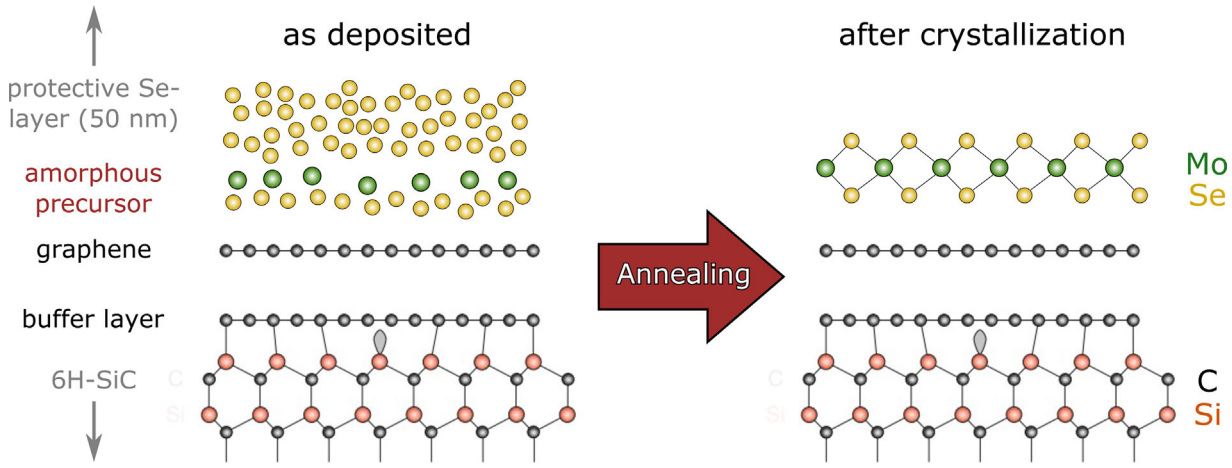

Figure 1. Schematic growth mechanism of monolayer $MoSe_2$ on epitaxial graphene on SiC(0001). First, an amorphous precursor of elemental Mo and Se is deposited on the graphene substrate and covered with a protective layer of 50 nm of elemental Se. The precursor self-assembles into crystalline $MoSe_2$ upon annealing and excess Se evaporates.

using a combination of conductive and non-conductive EPO-TEK H22 and H72 epoxy adhesives. Breaking off the top plate results in a clean cleave of the crystal, as demonstrated previously.[19]

After crystallization, the electronic and crystalline structure of the films were characterized using X-ray photoelectron spectroscopy (XPS), low-energy electron diffraction (LEED), atomic force microscopy (AFM), and Raman Spectroscopy. XPS and LEED

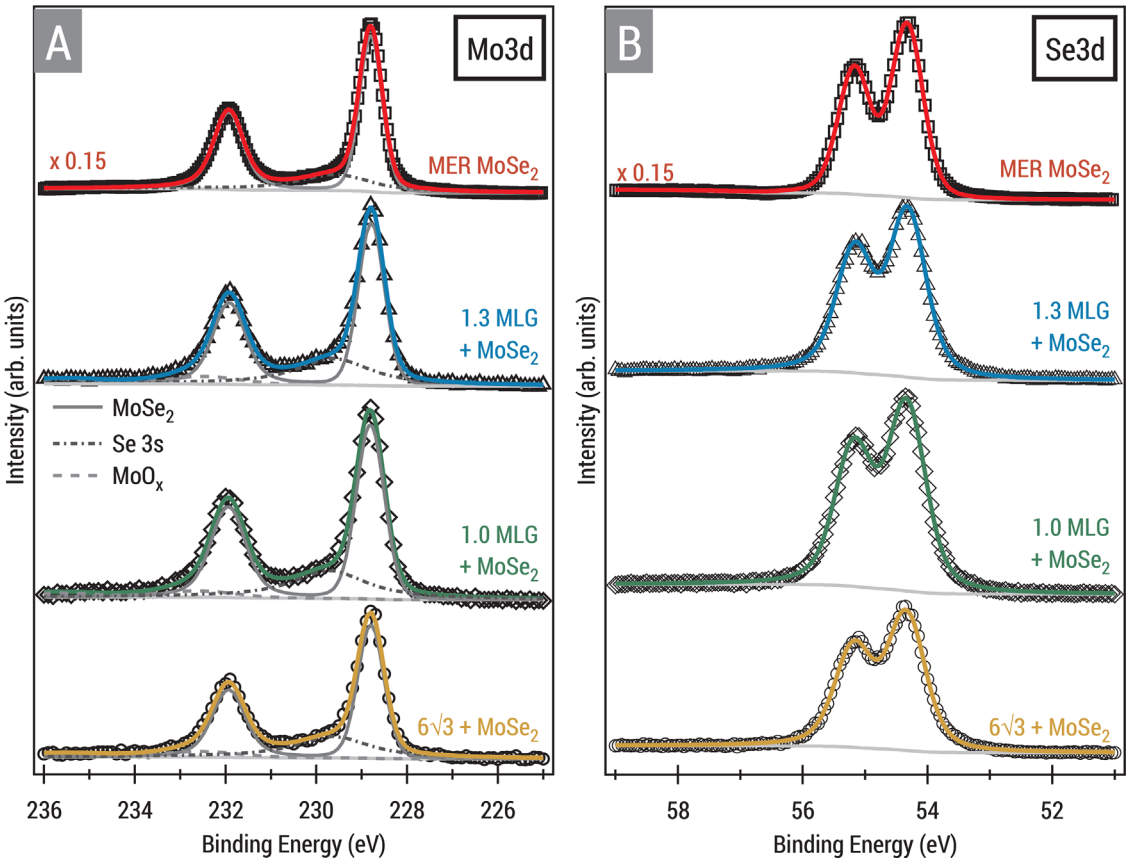

Figure 2. A) Mo3d and B) Se3d XPS core level spectra of $MoSe_2$ grown on epitaxial graphene in comparison to the bulk-like $MoSe_2$ reference sample grown with MER.

measurements were carried out in UHV below 3×10^{-10} mbar using Al K_α radiation from a SPECS XR50M X-ray source combined with a SPECS FOCUS 500 crystal monochromator and a SPECS Phoibos 150 MCD-9 hemispherical analyzer for XPS, and SPECS ErLEED 150 reverse view optics for LEED, respectively. AFM and Raman were performed ex situ on a Park Systems XE100 AFM and a LabRam HR800 Raman system, using 514.7 nm wavelength laser excitation and a 2400 grooves per mm grating.

3. Annealing Study

As is common in the MER synthesis, to form the desired product upon annealing the as-deposited precursor, an annealing study had to be carried out to optimize annealing temperature, time, and pressure. Because the peak positions of the Mo3d and Se3d core level signals as well as the Se:Mo ratio were later used to judge the quality of the annealed films, the reference sample was characterized by XPS before starting with the annealing study. To determine the Se:Mo ratio, the peak areas of the Mo3d and Se3d signals were determined from survey scans and corrected for their respective photoionization cross section σ as well as the kinetic energy-dependent transmission function T of the analyzer and electronic mean free path λ of the photoelectrons. σ-Values were calculated by Scofield[20] and λ was estimated using the TPP2M algorithm,[21] whereas T was determined experimentally.[22] Since the Se3s core level, which is located at a binding energy of about 230 eV is interfering with the Mo3d core level at 228.8 eV (as can be seen in the Mo3d core level spectra of the films in **Figure 2**a), the determined intensity of the Mo3d peak has to be corrected. The Se:Mo ratio can then be determined as follows

$$\mathrm{Se:Mo} = \frac{I_{\mathrm{Se3d}}}{\sigma_{\mathrm{Se3d}}\lambda_{\mathrm{Se3d}}T_{\mathrm{Se3d}}} \cdot \frac{\sigma_{\mathrm{Mo3d}}\lambda_{\mathrm{Mo3d}}T_{\mathrm{Mo3d}}}{I_{\mathrm{Mo3d}} - I_{\mathrm{Se3s}}} \quad (1)$$

where the intensity of the Se3s peak can be estimated from the intensity of the Se3d by using

$$I_{\mathrm{Se3s}} = I_{\mathrm{Se3d}} \cdot \frac{\sigma_{\mathrm{Se3s}}}{\sigma_{\mathrm{Se3d}}} \quad (2)$$

For the reference sample, this yields the expected Se:Mo ratio of 2.0 ± 0.3.

The annealing studies were carried out first by direct annealing of the samples with the precursors in UHV or in 750 mbar argon atmosphere. However, XPS spectra showed that instead of binding to the Mo atoms, the Se atoms were rapidly desorbing from the surface (see Figure S1, Supporting

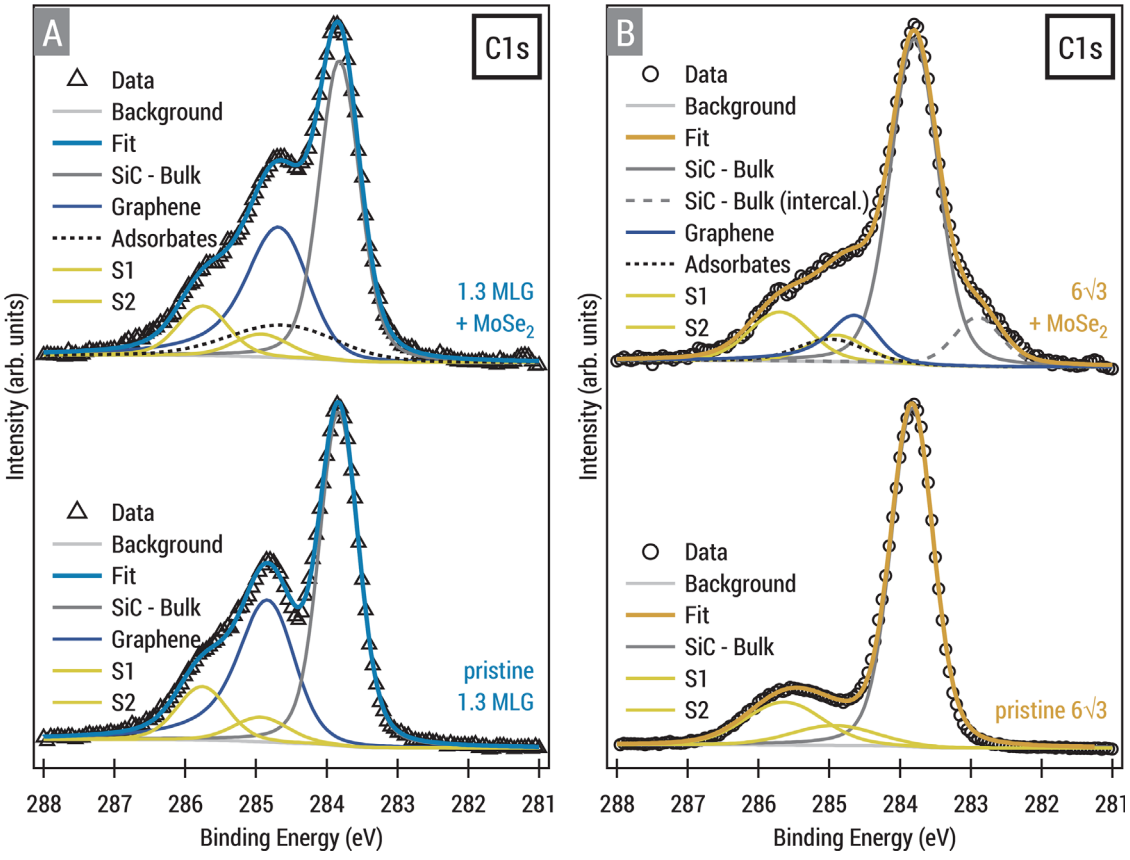

Figure 3. C1s core level spectra of (A) 1.3 MLG and (B) $6\sqrt{3}$ before (bottom row) and after (top row) growth of $MoSe_2$. See text for more information.

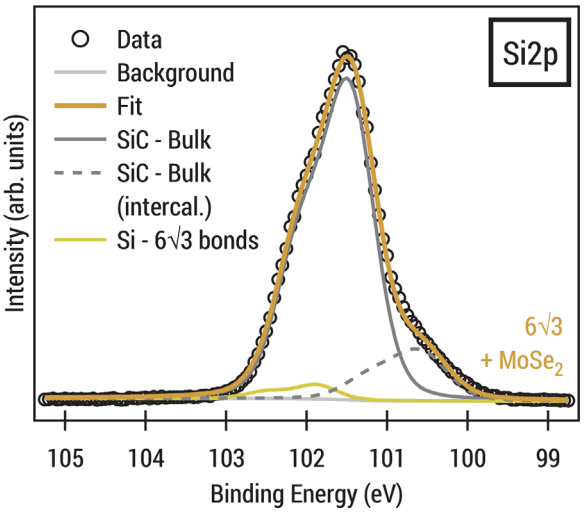

Figure 4. Si2p core level spectrum of $6\sqrt{3}$ after growth of $MoSe_2$. The spectrum shows a shoulder at lower binding energies, suggesting partial intercalation of the buffer layer.

Information). A piece of a hydrogen-etched SiC wafer was therefore placed on-top of the precursor to simulate increased pressure and thus trapping the Se atoms between the substrate and the top wafer during the reaction. This sandwich structure was mounted onto a sample holder and annealed in UHV at 450 °C for 1 h. After ex situ removal of the top wafer, samples were transferred back into UHV and characterized with XPS and LEED and afterwards with ex situ AFM and Raman spectroscopy. The Se:Mo ratio as determined from XPS survey spectra using Equation (1) for these samples ranged from 1.91 to 2.15, in good agreement with the desired target value of 2.0. Data from three different samples will be presented in the following, where $MoSe_2$ was successfully grown on a buffer layer ($6\sqrt{3}$) sample and two different monolayer graphene (MLG) samples with nominal graphene coverage as determined by XPS of 1.0 and 1.3 ML, respectively.

4. Results and Discussion

4.1. X-Ray Photoelectron Spectroscopy

XPS survey spectra showed the element specific signals of C, Si, Mo, and Se. Additionally, small amounts of oxygen could be detected as well as traces of SnO_2, which presumably contaminated the samples before or during the deposition of the precursors. High-resolution spectra of the Mo3d and Se3d core levels are shown in Figure 2a and b, respectively. The binding energy of the $Mo3d_{5/2}$ amounts to 228.8 eV and the $Se3d_{5/2}$ is located at 54.3 eV for the reference sample as well as for the films grown on epitaxial graphene and buffer layer, in good agreement with previous literature reports on $MoSe_2$.[6,7,9,23,24] This indicates the formation of $MoSe_2$. In the Mo3d spectra, the aforementioned Se3s peak can be found at 229.7 eV. At around 232.5 eV, a small second component can be found in the spectra that can be attributed to molybdenum oxide.[9] There are no signs of additional components in the Se spectrum, suggesting that after annealing all remaining Se atoms are bound to Mo.

Using the peak areas of the Se3d core level of $MoSe_2$ and the Si2p core level from the substrate, we estimated the average thickness of the $MoSe_2$ films. For the film grown on $6\sqrt{3}$, the layer thickness is ≈6.3 Å. On the MLG samples, this yields a thickness of 6.5 Å and 5.9 Å for 1.0 and 1.3 ML graphene, respectively. For bulk $MoSe_2$, the layer thickness is known to be 6.5 Å,[25] meaning that our samples show a coverage of 0.9–1.0 ML $MoSe_2$.

To probe the influence of the $MoSe_2$ growth on the graphene, the C1s core level was measured for all samples before and after the growth process. As can be seen from the bottom row in **Figure 3**, the pristine samples show multiple components, which can be assigned to carbon atoms in bulk SiC, two components S1

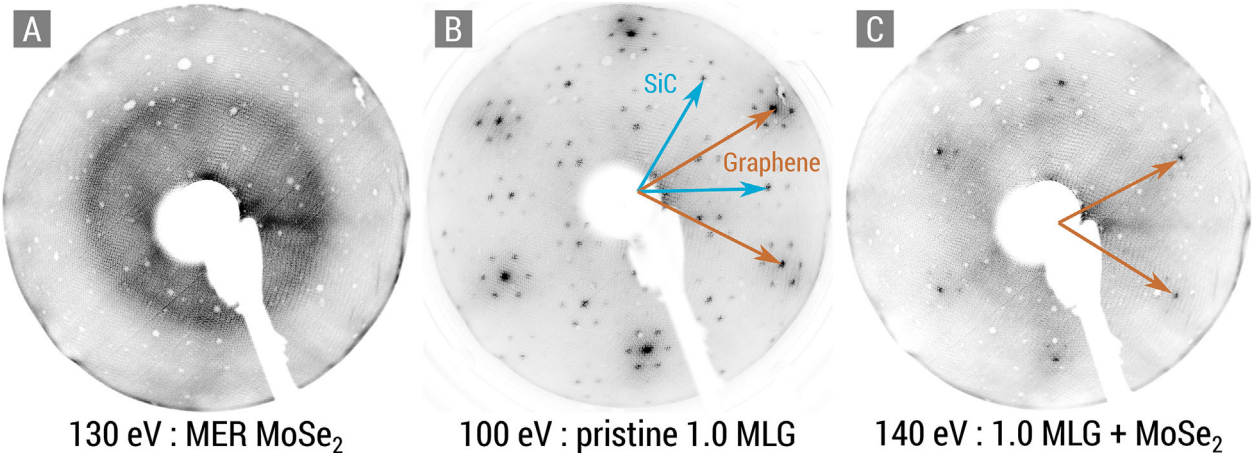

Figure 5. Low-energy electron diffraction patterns of (A) $MoSe_2$ reference sample showing a ring due to rotational disorder, (B) pristine 1.0 MLG sample showing spots corresponding to epitaxial graphene, SiC and the $(6\sqrt{3} \times 6\sqrt{3})R30°$ reconstuction of the buffer layer, and (C) 1.0 MLG sample covered with $MoSe_2$, where a faint ring can be seen along with the weak graphene spots.

and S2 of the buffer layer (which is still covalently bound to Si), as well as a graphene component for the MLG sample.[16] The top row shows the spectra of the same samples after the growth of $MoSe_2$. It should be noted that a background subtraction was carried out on the data to account for the presence of Se Auger peaks in the measured region. For the MLG sample (Figure 3a), the bulk and buffer layer components remain unchanged after the growth. The graphene component shows a slight shift to lower binding energies, indicating electron transfer from the graphene to the $MoSe_2$. The binding energy of the graphene peak is located at 284.53 eV, which is close to charge neutrality[26] with possibly a remaining slight n-type doping. An additional broad component centered at 284.6 eV is necessary to adequately fit the spectrum, which we assign to residual carbon on the surface.

The $6\sqrt{3}$ sample (Figure 3b) shows a more complex behavior. As can be seen, the SiC bulk signal shows a shoulder at lower binding energies after the growth process. The same can be seen from the corresponding Si2p core level (**Figure 4**). This is a sign of a partial intercalation of the buffer layer, which is partly converted to a quasi-freestanding graphene layer.[27,28] The new emerging SiC bulk component is shifted from its original position due to a change in band bending upon saturation of the bonds of the Si atoms at the interface.[29] Further support of this explanation is given by the presence of a graphene component at 284.52 eV in the C1s core level, which is not present in the spectrum of the pristine sample. Since no additional components in the Mo3d and Se3d spectra were observed for this sample, we assume that most likely residual oxygen is the intercalating element. For the MLG samples, the Si2p spectra (not shown) remain unchanged before and after growth of $MoSe_2$, consistent with the absence of an intercalated bulk component in the C1s spectra.

4.2. Low-Energy Electron Diffraction

Figure 5a shows a low-energy electron diffraction pattern of the bulk-like $MoSe_2$ reference sample. A ring is visible instead of distinct diffraction spots, owing to the turbostratic rotational disorder that is inherent to most products of the modulated elemental reactants synthesis.[13] The pristine MLG sample (Figure 5b) shows the diffraction spots from the SiC substrate and the graphene layer. Additional spots correspond to the $(6\sqrt{3} \times 6\sqrt{3})R30^\circ$ reconstruction from the buffer layer.[17] After the growth of $MoSe_2$ (Figure 5c), the diffraction spots from graphene are significantly attenuated but still visible. No clear diffraction pattern that stems from the $MoSe_2$ can be observed. However, a very faint ring structure can be seen, that might be tentatively assigned to the $MoSe_2$. This would suggest that the layers exist in very small and randomly rotated domains without an epitaxial relationship to the substrate, which would be consistent with the structure of the reference sample.

4.3. Atomic Force Microscopy

Representative AFM topography scans acquired after the growth process are shown in **Figure 6**. Images were adjusted so that terraces appear at equal height. The typical terraces from the SiC substrate are still clearly visible, as can be seen from the height profile inset in Figure 6b, where the underlying SiC step structure is indicated by a dashed line. Pristine $6\sqrt{3}$ and MLG samples usually show atomically flat terraces.[16] After the growth of the $MoSe_2$ layers, the terraces are densely covered with a grainy structure, indicating that the $MoSe_2$ films do not grow as a perfectly homogeneous layer but rather as a multitude of very small grains. This explanation is consistent with the LEED diffraction patterns, which suggest a large number of randomly orientated $MoSe_2$ domains. The crystalline orientation of a single grain is, however, not accessible with the experimental

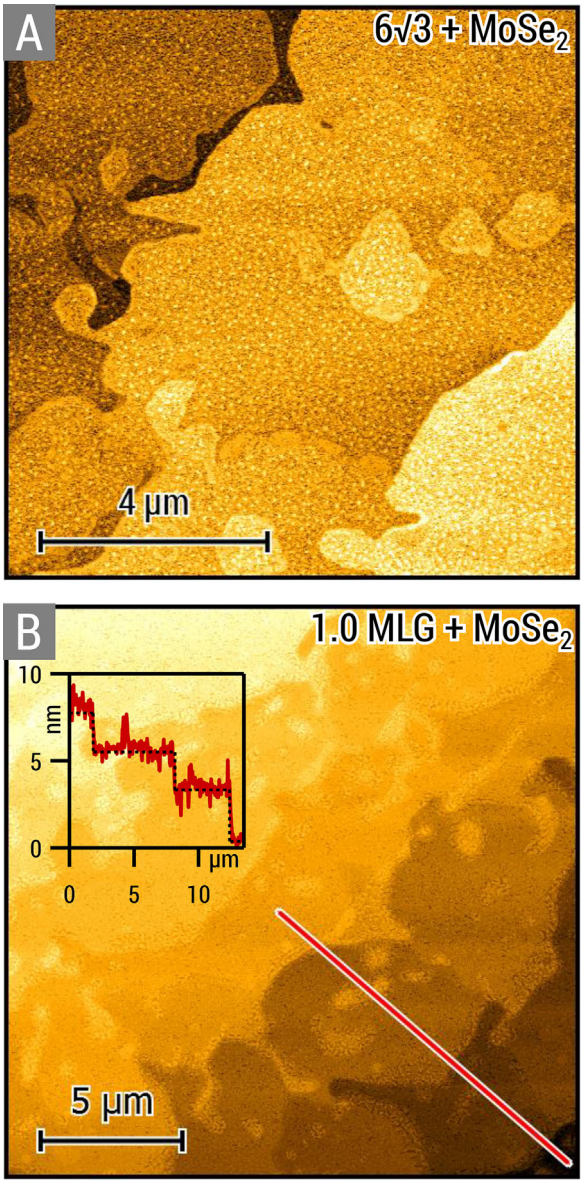

Figure 6. AFM topography images of the as-grown $MoSe_2$ films on (A) $6\sqrt{3}$ and (B) 1.0 ML graphene. The z-scale ranges from 0 to (A) 8.5 nm, and (B) 15.5 nm, respectively. The inset shows a height profile along the marked line, with the SiC steps of the MLG substrate added as guide to the eye with a dashed line.

setup. The films grown on buffer layer and MLG samples appear to be similar in structure, illustrating that the MER synthesis may be applicable without the restriction to a specific substrate. While grain sizes so far do not challenge the micrometer-sized flakes grown from CVD approaches,[23,30] they seem to compare well with films grown by conventional MBE techniques which are in the range of several tens of nanometers.[8,10,31]

4.4. Raman Spectroscopy

Figure 7 shows Raman spectra collected on the samples in different energy regions. Spectra on a pristine buffer layer were collected to be used as a reference and for background correction. To eliminate the contributions of the SiC substrate and the buffer layer to the spectra in Figure 7a and b, the spectrum of the pristine buffer layer sample was substracted.

A region containing the peaks corresponding to $MoSe_2$ is shown in Figure 7a. The bulk-like reference sample shows a very sharp peak at 242.8 cm^{-1}, which can be assigned to the A_{1g} mode.[32,33] This peak shows a slight asymmetry, which could be due to the nanocrystalline structure of MER-grown samples, as asymmetric Raman line shapes have been reported for nanostructured materials.[34] The two less intense peaks at 169.2 and 285.8 cm^{-1} can be assigned to the E_{1g} and $E^1{}_{2g}$ modes, respectively.[32,33] At 351.4 cm^{-1}, an additional small signal is observed, which Nam et al.[32] assigned to the Raman forbidden $A^2{}_{2u}$ mode. Tonndorf et al.[33] observed a signal in this energy range as well for few layer $MoSe_2$ and assigned it to the $B^1{}_{2g}$ mode, but claimed it should be inactive in a bulk material. Another very weak signal marked with an * can be found at 314.5 cm^{-1}. According to Nam et al.,[32] this can be assigned to multiple-phonon scattering of the E_{1g} and LA branch or the two-phonon frequency of the B_{2g} branch. If one looks at the spectra of the thin layers grown on epitaxial graphene, only three Raman signals can be resolved. We again assign the most intense peak at 239.0 cm^{-1} to the A_{1g} mode. While the A_{1g} mode is redshifted from the bulk, the $E^1{}_{2g}$ mode shows a blue shift to 289.9 cm^{-1}. These values are within 2 cm^{-1} of the values reported by Ugeda et al.[8] for MBE grown $MoSe_2$ on bilayer graphene on 6H-SiC(0001). At 253.8 cm^{-1}, we can observe an additional peak emerging that is not present in the bulk sample and was not reported for $MoSe_2$ grown by MBE on epitaxial graphene.[8,9] We tentatively assign this peak to the two-phonon energy of the $E^2{}_{2g}$ mode, which can be found at 249.4 cm^{-1} in single-crystalline bulk 2H-$MoSe_2$.[32] In principle, Raman spectroscopy is sensitive to the thickness of $MoSe_2$, as a small splitting of the A_{1g} mode was observed for 3–5 layers of mechanically exfoliated[33] and CVD grown[30] $MoSe_2$. However, for our samples it was not possible to resolve this experimentally.

Figure 7b and c show the G and 2D Raman signals corresponding to the epitaxial graphene layers. Since the buffer layer also gives a signal in the spectral region of the G band,[35] the spectrum of a pristine buffer layer was subtracted to account for the background of the substrate. For MLG samples covered by $MoSe_2$, we find the position of the G and 2D band at 1590 cm^{-1} and 2711–2715 cm^{-1} by fits of single Lorentzians, which is in the range reported for pristine MLG samples by Fromm.[36] Both signals show a blue shift compared to undoped and unstrained exfoliated graphene (dashed line). This shift can be attributed to a combination of compressive strain and charge on the epitaxial graphene layer.[37–39] While a model was developed to separate the contributions of strain and charge on the G and 2D positions and which could give an estimate of the charge carrier concentration in quasi-freestanding epitaxial graphene,[37] this unfortunately does not apply to MLG due to

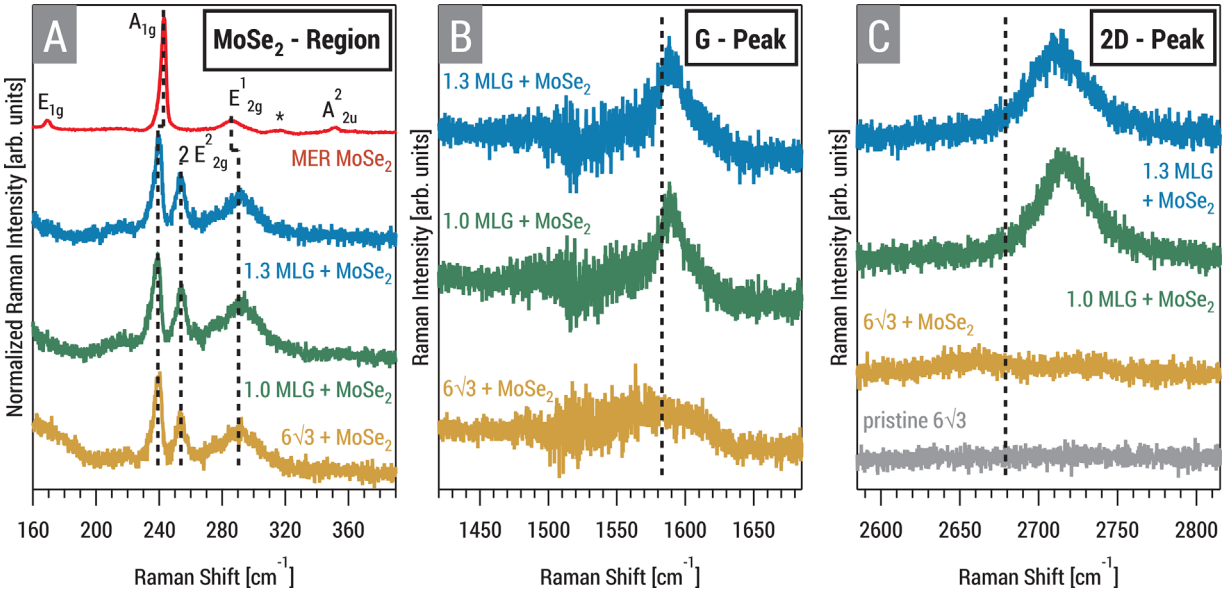

Figure 7. Raman spectra of $MoSe_2$ grown on epitaxial graphene on SiC: A) Raman signals corresponding to $MoSe_2$ in comparison to the bulk-like sample. B) Graphene G-peak and C) graphene 2D-peak of the graphene substrates. Dashed lines indicate the positions for unstrained and uncharged graphene.

potential differences in the phononic structure,[36] so no conclusions on a potential charge transfer from $MoSe_2$ can be drawn from Raman. The buffer layer sample showed a partial intercalation in the XPS spectra, suggesting the formation of areas with quasi-freestanding graphene on the surface. Consequently, a small signal can be observed at the position of the G band in the Raman spectrum. In the region of the 2D band, a small bump centered around 2664 cm^{-1} can be seen, which is close to the position reported for H-intercalated QFMLG.[40] We conclude that a small portion of the buffer layer is intercalated, consistent with the XPS results. It should be noted that, for all samples, no significant intensity of the D-Peak (which is usually centered around 1350 cm^{-1}) could be observed. The D-Peak intensity is usually related to defects in graphene,[41] and its absence indicates that the MER growth of $MoSe_2$ does not negatively effect the quality of the epitaxial graphene substrate.

5. Conclusions

We prepared thin layers of $MoSe_2$ on top of epitaxial graphene and buffer layer by annealing of an amorphous precursor consisting of elemental Mo and Se. By means of XPS and Raman spectroscopy, the as-grown films could be identified as the targeted $MoSe_2$ thin films, where XPS suggests an average film thickness of about one monolayer. From electron diffraction, we can tentatively presume that the films show small, randomly rotated domains, as is common for products of the MER synthesis. AFM topography scans show that the graphene terraces are covered by a grainy structure, consistent with the conclusion from LEED experiments. XPS and Raman spectroscopy suggest that the growth of $MoSe_2$ using the MER synthesis does not significantly change the properties of the underlying graphene monolayer aside from a small charge transfer. Amorphous precursors may therefore provide a tool to grow numerous and more complex heterostructures, consisting of different types of layers, on epitaxial graphene to be used for fundamental research and potential applications.

Supporting Information

Supporting Information is available from the Wiley Online Library or from the author.

Acknowledgment

The research leading to these results was supported by the European Union in the framework of the Graphene Flagship under contact no. 696656.

Conflict of Interest

The authors declare no conflict of interest.

Keywords

epitaxial graphene, modulated elemental reactants, $MoSe_2$, transition metal dichalcogenides

Received: June 14, 2018
Revised: August 6, 2018
Published online: September 11, 2018

[1] A. C. Ferrari, F. Bonaccorso, V. Fal'ko, K. S. Novoselov, S. Roche, P. Bøggild, S. Borini, F. H. L. Koppens, V. Palermo, N. Pugno, J. A. Garrido, R. Sordan, A. Bianco, L. Ballerini, M. Prato, E. Lidorikis, J. Kivioja, C. Marinelli, T. Ryhänen, A. Morpurgo, J. N. Coleman, V. Nicolosi, L. Colombo, A. Fert, M. Garcia-Hernandez, A. Bachtold, G. F. Schneider, F. Guinea, C. Dekker, M. Barbone, Z. Sun, C. Galiotis, A. N. Grigorenko, G. Konstantatos, A. Kis, M. Katsnelson, L. Vandersypen, A. Loiseau, V. Morandi, D. Neumaier, E. Treossi, V. Pellegrini, M. Polini, A. Tredicucci, G. M. Williams, B. H. Hong, J. H. Ahn, J. M. Kim, H. Zirath, B. J. van Wees, H. van der Zant, L. Occhipinti, A. D. Matteo, I. A. Kinloch, T. Seyller, E. Quesnel, X. Feng, K. Teo, N. Rupesinghe, P. Hakonen, S. R. T. Neil, Q. Tannock, T. Löfwander, J. Kinaret, *Nanoscale* **2015**, *7*, 4598.
[2] M. Chhowalla, H. S. Shin, G. Eda, L. J. Li, K. P. Loh, H. Zhang, *Nature Chem.* **2013**, *5*, 263.
[3] A. B. Kaul, *J. Mater. Res.* **2014**, *29*, 348.
[4] A. Kuc, T. Heine, A. Kis, *MRS Bull.* **2015**, *40*, 577.
[5] A. K. Geim, I. V. Grigorieva, *Nature* **2013**, *499*, 419.
[6] Z. Liu, N. Li, H. Zhao, Y. Du, *J. Mater. Chem. A* **2015**, *3*, 19706.
[7] G. W. Shim, K. Yoo, S. B. Seo, J. Shin, D. Y. Jung, I. S. Kang, C. W. Ahn, B. J. Cho, S. Y. Choi, *ACS Nano* **2014**, *8*, 6655.
[8] M. M. Ugeda, A. J. Bradley, S. F. Shi, F. H. da Jornada, Y. Zhang, D. Y. Qiu, W. Ruan, S. K. Mo, Z. Hussain, Z. X. Shen, F. Wang, S. G. Louie, M. F. Crommie, *Nature Mater.* **2014**, *13*, 1091.
[9] S. Vishwanath, X. Liu, S. Rouvimov, P. C. Mende, A. Azcatl, S. McDonnell, R. M. Wallace, R. M. Feenstra, J. K. Furdyna, D. Jena, H. G. Xing, *2D Mater.* **2015**, *2*, 024007.
[10] M. T. Dau, M. Gay, D. D. Felice, C. Vergnaud, A. Marty, C. Beigné, G. Renaud, O. Renault, P. Mallet, T. L. Quang, J. Y. Veuillen, L. Huder, V. T. Renard, C. Chapelier, G. Zamborlini, M. Jugovac, V. Feyer, Y. J. Dappe, P. Pochet, M. Jamet, *ACS Nano* **2018**, *12*, 2319.
[11] D. C. Johnson, *Curr. Opin. Solid State Mater. Sci.* **1998**, *3*, 159.
[12] M. Noh, C. D. Johnson, M. D. Hornbostel, J. Thiel, D. C. Johnson, *Chem. Mater.* **1996**, *8*, 1625.
[13] M. Beekman, C. L. Heideman, D. C. Johnson, *Semicond. Sci. Technol.* **2014**, *29*, 064012.
[14] D. M. Hamann, E. C. Hadland, D. C. Johnson, *Semicond. Sci. Technol.* **2017**, *32*, 093004.
[15] M. Esters, M. B. Alemayehu, Z. Jones, N. T. Nguyen, M. D. Anderson, C. Grosse, S. F. Fischer, D. C. Johnson, *Angew. Chem. Int. Ed.* **2015**, *54*, 1130.
[16] K. V. Emtsev, A. Bostwick, K. Horn, J. Jobst, G. L. Kellogg, L. Ley, J. L. McChesney, T. Ohta, S. A. Reshanov, J. Röhrl, E. Rotenberg, A. K. Schmid, D. Waldmann, H. B. Weber, T. Seyller, *Nature Mater.* **2009**, *8*, 203.
[17] K. V. Emtsev, F. Speck, T. Seyller, L. Ley, J. D. Riley, *Phys. Rev. B* **2008**, *77*, 155303.
[18] M. Ostler, F. Speck, M. Gick, T. Seyller, *Phys. Status Solidi B* **2010**, *247*, 2924.
[19] F. Göhler, G. Mitchson, M. B. Alemayehu, F. Speck, M. Wanke, D. C. Johnson, T. Seyller, *J. Phys.: Condens. Matter* **2018**, *30*, 055001.
[20] J. Scofield, *J. Electron Spectrosc. Relat. Phenom.* **1976**, *8*, 129.
[21] S. Tanuma, C. J. Powell, D. R. Penn, *Surf. Interface Anal.* **1994**, *21*, 165.

[22] S. Peter, F. Speck, M. Lindner, T. Seyller, *Vacuum* **2017**, *138*, 191.
[23] X. Wang, Y. Gong, G. Shi, W. L. Chow, K. Keyshar, G. Ye, R. Vajtai, J. Lou, Z. Liu, E. Ringe, B. K. Tay, P. M. Ajayan, *ACS Nano* **2014**, *8*, 5125.
[24] W. A. Abdallah, A. E. Nelson, *J. Mater. Sci.* **2005**, *40*, 2679.
[25] Y. Zhang, T. R. Chang, B. Zhou, Y. T. Cui, H. Yan, Z. Liu, F. Schmitt, J. Lee, R. Moore, Y. Chen, H. Lin, H. T. Jeng, S. K. Mo, Z. Hussain, A. Bansil, Z. X. Shen, *Nature Nanotechnol.* **2014**, *9*, 111.
[26] G. Wertheim, P. V. Attekum, S. Basu, *Solid State Commun.* **1980**, *33*, 1127.
[27] M. Ostler, F. Fromm, R. J. Koch, P. Wehrfritz, F. Speck, H. Vita, S. Böttcher, K. Horn, T. Seyller, *Carbon* **2014**, *70*, 258.
[28] S. Mammadov, J. Ristein, R. J. Koch, M. Ostler, C. Raidel, M. Wanke, R. Vasiliauskas, R. Yakimova, T. Seyller, *2D Mater.* **2014**, *1*, 035003.
[29] T. Seyller, *J. Phys.: Condens. Matter* **2004**, *16*, S1755.
[30] J. C. Shaw, H. Zhou, Y. Chen, N. O. Weiss, Y. Liu, Y. Huang, X. Duan, *Nano Res.* **2014**, *7*, 511.
[31] M. T. Dau, C. Vergnaud, A. Marty, F. Rortais, C. Beigné, H. Boukari, E. Bellet-Amalric, V. Guigoz, O. Renault, C. Alvarez, H. Okuno, P. Pochet, M. Jamet, *Appl. Phys. Lett.* **2017**, *110*, 011909.
[32] D. Nam, J. U. Lee, H. Cheong, *Sci. Rep.* **2015**, *5*, 17113.
[33] P. Tonndorf, R. Schmidt, P. Böttger, X. Zhang, J. Börner, A. Liebig, M. Albrecht, C. Kloc, O. Gordan, D. R. T. Zahn, S. M. de Vasconcellos, R. Bratschitsch, *Opt. Express* **2013**, *21*, 4908.
[34] R. Kumar, G. Sahu, S. K. Saxena, H. M. Rai, P. R. Sagdeo, *Silicon* **2014**, *6*, 117.
[35] F. Fromm, M. H. Oliveira, Jr., A. Molina-Sánchez, M. Hundhausen, J. M. J. Lopes, H. Riechert, L. Wirtz, T. Seyller, *New J. Phys.* **2013**, *15*, 043031.
[36] F. Fromm, Raman-Spektroskopie an epitaktischem Graphen auf Siliziumkarbid (0001), *Ph.D. Thesis*, Technische Universität Chemnitz, Chemnitz, Germany **2014**.
[37] F. Fromm, P. Wehrfritz, M. Hundhausen, T. Seyller, *New J. Phys.* **2013**, *15*, 113006.
[38] J. Röhrl, M. Hundhausen, K. V. Emtsev, T. Seyller, L. Ley, *Mater. Sci. Forum* **2009**, *600–603*, 567.
[39] J. Röhrl, M. Hundhausen, F. Speck, T. Seyller, *Mater. Sci. Forum* **2010**, *645–648*, 603.
[40] F. Speck, J. Jobst, F. Fromm, M. Ostler, D. Waldmann, M. Hundhausen, H. B. Weber, T. Seyller, *Appl. Phys. Lett.* **2011**, *99*, 122106.
[41] L. G. Cançado, A. Jorio, E. H. M. Ferreira, F. Stavale, C. A. Achete, R. B. Capaz, M. V. O. Moutinho, A. Lombardo, T. S. Kulmala, A. C. Ferrari, *Nano Lett.* **2011**, *11*, 3190.